REVISTA MATÉRIA V.29 N.3
ISSN 1517-7076 articles e20240374, 2024

BN-TiO_2 multilayer coating on AZ91 for enhanced corrosion performance in marine environments

Emrah Meletlioğlu[1], Onur Çomakli[2]

[1]Ataturk University, Faculty of Engineering, Department of Mechanical Engineering. 25242, Erzurum, Turkey.

[2]Erzurum Technical University, Faculty of Engineering and Architecture, Department of Mechanical Engineering. 25240, Erzurum, Turkey.

e-mail: emrahmeletli@atauni.edu.tr, onur.comakli@erzurum.edu.tr

ABSTRACT

Magnesium alloys have recently been used in marine applications due to an attractive combination of low density and high strength/weight/ratio. However, the corrosion resistance of magnesium alloys should be improved for practical applications. In this study, BN-TiO_2 multilayer films were deposited with different numbers of bilayers (2 and 4) on AZ91 magnesium alloys to enhance the corrosion resistance of magnesium alloys in marine environments. The microstructure and wettability properties of uncoated and multilayer film-coated alloys were comparatively investigated via XRD, SEM, AFM, and contact angle measurement systems. The corrosion performance of uncoated and coated samples has also been evaluated using electrochemical polarization and impedance measurements in artificial seawater. The corrosion performance values of multilayer film-coated alloys were better than the uncoated alloy values. Corrosion resistance and hydrophobicity of coated samples also increased with the number of bilayers owing to the smaller grain size, increased layered interfaces, and high structural density.

Keywords: AZ91 magnesium alloys; Multilayer film; Corrosion; Artifical seawater.

1. INTRODUCTION

Magnesium alloys, known for their exceptional properties, such as low density and high specific strength, have been extensively utilized in the aerospace, automotive, and 3C industries. However, the application and development of magnesium alloys are constrained due to their inadequate corrosion resistance, particularly in aggressive corrosive environments [1, 2]. To expedite the assessment of the corrosion resistance of magnesium alloys, numerous studies have been conducted to simulate their corrosion behavior, including immersion tests and salt spray experiments [3, 4]. However, the corrosion behavior of Mg alloys in actual service atmospheric environments is inconsistent with that in the accelerated simulated corrosion tests mentioned above [5, 6]. It is well known that Mg alloys are mainly exposed to atmospheric environments during practical application. In recent years, many studies have been conducted on the corrosion behavior of magnesium alloys in marine and industrial environments [7, 8]. In addition, this alloy's poor corrosion resistance can severely limit its applications in the marine field, where chloride concentrations are much higher than those in a 3.5 wt percent NaCl solution [9, 10]. To ensure long-term serviceability, magnesium alloys must have good corrosion resistance. Therefore, coating techniques like chemical vapor deposition, plasma spray deposition, anodic oxidation, physical vapor deposition, and ion implantation are attracting increasing attention regarding solutions [11, 12].

Protective ceramic films formed by physical vapor deposition, a well-known coating technique, are widely used to improve properties such as hardness and wear resistance of alloys and reduce friction. Multilayer films, for instance, have advantages over conventional films when it comes to enhancing characteristics like corrosion resistance, hardness, modulus, and elastic modulus. Regarding corrosion prevention, the multilayer ceramic film keeps harmful substances from the metal surface while preventing pores, cracks, and other defects caused by the material structure [13, 14]. Previous studies have shown that multilayer coatings applied using the physical vapor deposition (PVD) process improve magnesium alloys' corrosion performance, surface hardness, and wear resistance. For example, WU *et al.* [15] investigated the corrosion resistance of an Al_2O_3/Al and Al_2O_3/Ti multilayer. They found that the maximum corrosion resistance was reached for Al_2O_3/Al multilayer-coated samples more significantly than the substrate materials. The effect of the TiAlN multilayer films on the

Corresponding Author: Emrah Meletlioğlu Received on 23/06/2024 Accepted on 15/07/2024

DOI: https://doi.org/10.1590/1517-7076-RMAT-2024-0374

hardness, thickness, and corrosion performance of AZ91 magnesium alloys was examined by LIANG *et al.* [16]. They reported that a multilayer film coated on a magnesium substrate improved surface hardness and enhanced corrosion resistance. ZHANG *et al.* [17] prepared a Hf/Si_3N_4 multilayer film on AZ91 materials via magnetron sputtering, and test results showed that the multilayer-coated magnesium samples exhibited higher surface hardness, reduced its friction coefficient and improvement of the wear resistance compared with the untreated specimens.

Boron nitride (BN) nanoparticles in ceramic coatings are being examined for their unique characteristics, including chemical stability and excellent corrosion resistance [18, 19]. These nano-sized particles can improve the durability and protection of the AZ91 magnesium alloy, making it more corrosion-resistant even in seawater. Even so, studies have shown that doping these nanoparticles into the matrix can reduce the degradation that occurs during the aging process of metallic alloys [20, 21]. Besides BN coatings, ceramic TiO_2 coatings have been shown to have desirable physical features such as low coefficient of friction and superior corrosion resistance [22]. Previous research has demonstrated that TiO_2 coatings improve not only corrosion resistance but also the surface hardness of substrates [23, 24]. However, the lack of studies in which BN-TiO_2 multilayer coating was exposed to corrosion in saltwater environments and the idea of using the properties of the multilayer coating to improve the mechanical properties of the AZ91 magnesium alloy inspired the presented research.

Therefore, this study's BN/TiO_2 multilayer ceramic coatings were formed on the AZ91 marine equipment material using a physical vapor deposition (PVD) system. All sample's surface structures and mechanical properties were examined, and their corrosion behaviors in artificial seawater solution were investigated and compared.

2. MATERIALS AND METHODS

The chemical composition of the commercially available magnesium alloy AZ91 is illustrated in Table 1. It was provided by the National Metallurgical Laboratory, India, to be used as the substrate.

The samples were in the form of square prisms measuring 20 × 20 × 4 mm. All samples were cleaned using 80–2000 grit SiC paper and polished with 0.3 µm Al_2O_3 powder to achieve a uniformly smooth surface. The samples were washed with ethyl alcohol and dried immediately. The BN-TiO_2 multilayer films were deposited on an AZ91 magnesium alloy using a Nanovak NVTS 400 PVD system, aiming for 99.999 purity for BN and TiO_2. Two sets of BN-TiO_2 multilayer ceramic films were deposited on the substrates, varying the number of bilayers (4 and 8) and keeping the total thickness the same. Each double layer consisted of a TiO_2 layer, which was applied first, followed by a BN layer. The coating parameters are given in Table 2.

Table 1: Chemical composition of AZ91 (wt.%).

Mg	Al	Zn	Mn	Fe	Cu
Balance	8.63 wt%	0.59 wt%	0.17 wt%	< 0.05 wt%	< 0.05 wt%

Table 2: Process parameters of coating.

PARAMETERS	VALUES
Deposition pressure (mTorr)	10
Deposition temperature (ºC)	45
RF power (W)	BN TiO_2 120 120
Deposition rates (Aº/s)	BN TiO_2 0.2 0.2
Bilayer numbers	2 bilayers 4 bilayers
Deposition time of BN targets (min)	416 208
Deposition time of TiO_2 targets (min)	416 208
Total deposition time (min)	1664 1664

After the deposition of the multilayer films, amorphous films appeared. The amorphous multilayer films were then heated to 550°C in a quartz tube furnace for 120 min. to initiate crystallization. The phase structures of the materials were examined using an X-ray diffraction device (GNR Explorer, 40 kV, 40 mA) with Cu Kα radiation (λ = 1.54187 Å). Scanning electron microscopy (SEM) was used to create cross-sectional images of the coatings and images of wear scars after wear tests. The grain size of the samples coated with the multilayer film was also measured using an atomic force microscope (AFM). The contact angles (CA) were detected by utilizing the sessile drop method with a contact angle meter (Attension Theta Flex) to determine measurements of wettability of the coated sample surfaces. The CA values were obtained from water droplets (5 µl) at seven different positions on surface. The electrochemical measurements were carried out with a Gamry Series G 750 Potentiostat/Galvanostat. For the corrosion tests, an artificial seawater solution was prepared and used to replicate seawater prepared by the ASTM D1141 standard [25]. Graphite served as the counter electrode, Ag/AgCl as the reference electrode, and the prepared sample with an exposed surface of 0.38 cm^2 as the working electrode in 130 ml of artificial seawater. This was carried out with a conventional three-compartment cell. Electrochemical impedance spectroscopy (EIS) was measured at the open circuit potential (OCP) with a frequency range of 100 kHz to 0.01 Hz and an AC amplitude of 10 mV. Using a suitable fitting approach created by the Zsimpwin program, the experimental results were interpreted based on an equivalent circuit diagram. The polarization curves covering the potential range from –1 to +2 VRef were recorded at a 1 mV s^{-1} scan rate. The potentiodynamic polarization and EIS tests were repeated at least three times to ensure that the test results were consistent.

3. RESULTS AND DISCUSSION

3.1. Microstructures

The XRD patterns of the uncoated and multilayer BN-TiO_2 film-coated AZ91 alloys are shown in Figure 1. Mg peaks (JCPDF code: 96-900-8507) were detected in uncoated AZ91 alloy, as seen in Figure 1. After the PVD coating process, new peaks appeared in the XRD pattern of multilayer film-coated alloys, including BN-boron nitride (JCPDF code: 96-201- 6174), TiO_2-anatase (JCPDF code: 96-720-6076). The increase in the double layers resulted in a gradual rise in the BN and TiO_2 peaks. Moreover, the shift of these peaks towards higher angles is thought to be caused by compressive residual stresses in the multilayered coating systems [26]. Multilayer films containing 8 bilayers were observed to demonstrate stress relief, which is evident through the peak shifting towards higher angles compared to films with 4 bilayers. The stress development in the BN and TiO_2 peak positions is characterized by a gradual and pronounced symmetric broadening and a rise in their intensity in BN/TiO_2 multilayer coatings. Potential stress relief can be observed due to the increase in the number of interfaces when the number of bilayers, n, is increased from 2 to 4—furthermore, individual layers with reduced thickness exhibit lower residual stress.

SEM photos of cross-sections of multilayer film with 2 and 4 bilayers are shown in Figure 2. According to Figure 2a, distinct BN and TiO_2 layers are observed in the structure of the multilayer film with 2 bilayers.

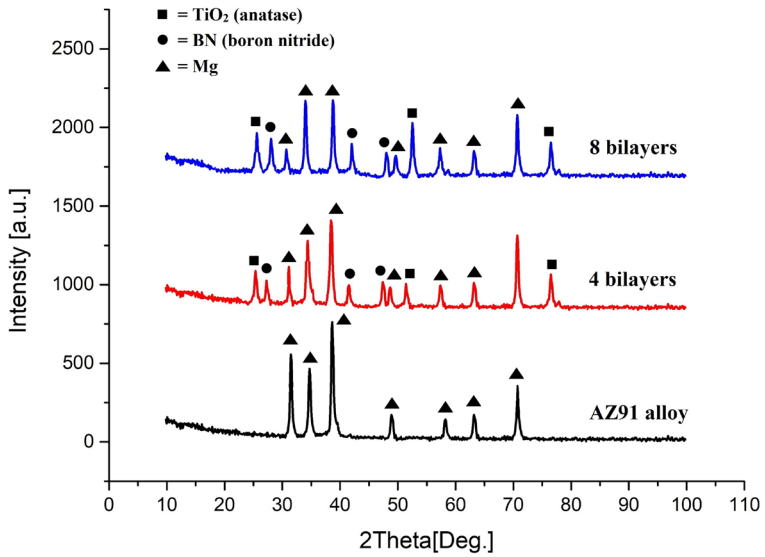

Figure 1: XRD results of AZ91 magnesium alloy.

On the other hand, when the structure of a multilayer film with 4 bilayers is examined, it has a more uniform and integrated structure (Figure 2b). This occurs because columnar growth is inhibited during TiO_2 deposition, forming a thin and dense microstructure. EDX analyses of full area-1 and full area-2 are shown in Figure 2 (c–d). As shown in Figure 2(c), B and N were detected on the surface of the BN layer, which indicates that BN film was deposited in a multilayer system. According to Figure 2 (d), Ti and O were obtained from the TiO_2 layer. This proves that the TiO_2 layer is inside the multilayer film.

Atomic Force Microscopy (AFM) was employed to assess the grain size of BN/TiO_2 multilayer film coatings on the substrate, correlating it with the increase in the number of bilayers. A reduction in grain size was likely observed due to higher bilayer counts, resulting in decreased bilayer thickness, which subsequently influenced grain growth within individual layers, as illustrated in Figure 3. It can be said that the grain size in multilayer films decreases with the increase in the number of bilayers due to the reduction in individual bilayer thickness. When more bilayers are deposited, each bilayer becomes thinner, limiting the space available for grain growth within each layer. This restriction results in smaller grains forming as the number of bilayers increases [27].

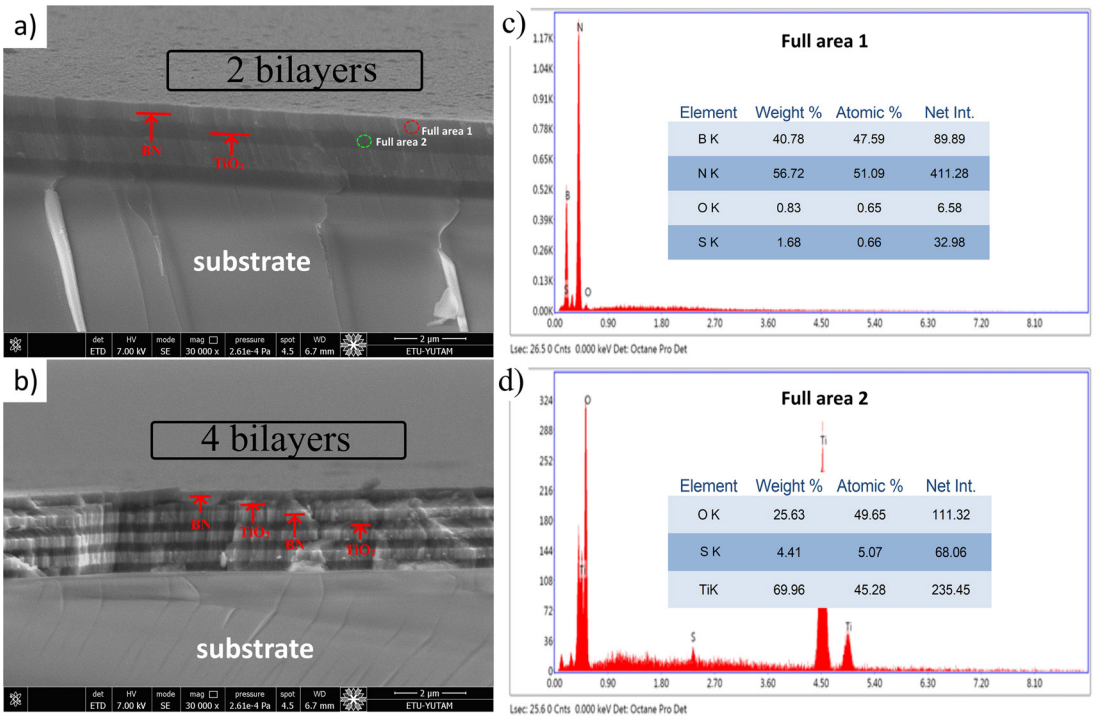

Figure 2: Cross-section SEM micrographs and EDS results observed for multilayer films: (a) and (c) 2 bilayers; (b) and (d) 4 bilayers.

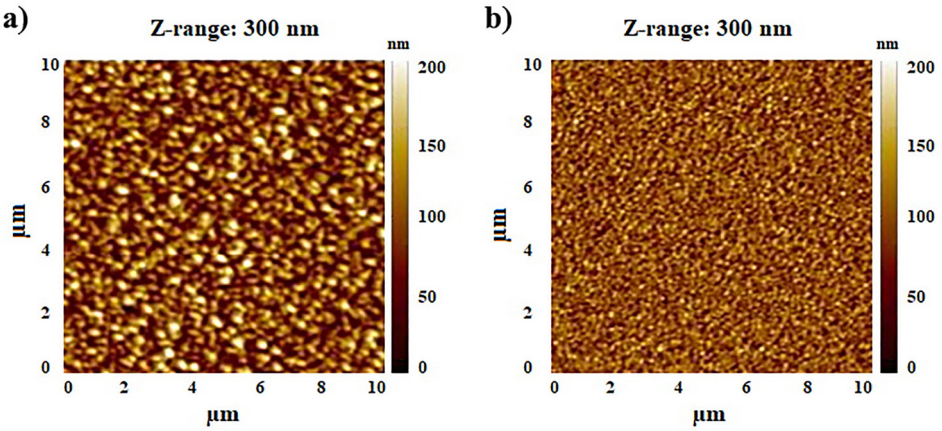

Figure 3: Semi-contact mode AFM photos of multilayer films: (a) 2 bilayers; (b) 4 bilayers.

Figure 4 illustrates the outcomes of the contact angle measurements conducted on the samples. Upon examination of the figure, it becomes evident that all of the samples exhibit hydrophobic properties, as the angle formed with the surface exceeds 90 degrees. The results indicate that the sample consisting of a multilayer film with 4 bilayers showcases the highest level of water repellency, with an angle of approximately 125°. Additionally, it can be inferred that the number of bilayers influences the surface characteristics of BN/TiO_2 multilayer films, leading to decreased wettability. Moreover, the observed changes in wettability in the samples coated with multilayers can be attributed to variations in surface roughness. The relationship between contact angle and surface roughness is complex and can be understood through the Wenzel and Cassie-Baxter models, which describe how surface roughness affects wetting behavior. According to the Wenzel model, when a liquid droplet spreads on a rough surface, the actual area of contact between the liquid and the surface increases. This model suggests that surface roughness enhances the wettability of hydrophilic surfaces and decreases the wettability of hydrophobic surfaces. It is well-established that an increase in the surface roughness of a material leads to a decrease in contact angle with water, resulting in enhanced hydrophilicity due to the liquid infiltrating the air pockets within the surface asperities. Consequently, according to AFM results, multilayer film with 4 bilayers exhibits the highest contact angles, attributed to their minimal surface roughness [28].

3.2. Corrosion performance

Corrosion tests were conducted to investigate the influence of multilayer films on the corrosion performance of AZ91 alloys in artificial seawater. Figure 5 shows the Tafel polarization curves for the uncoated and multilayer BN-TiO_2 film-coated AZ91 alloys.

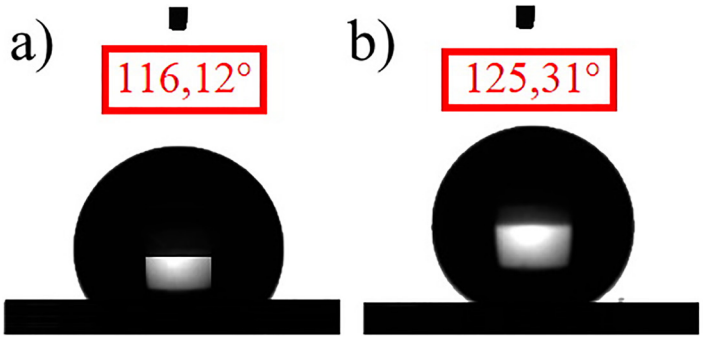

Figure 4: Contact angle measurement results of the samples: (a) 2 bilayers; (b) 4 bilayers.

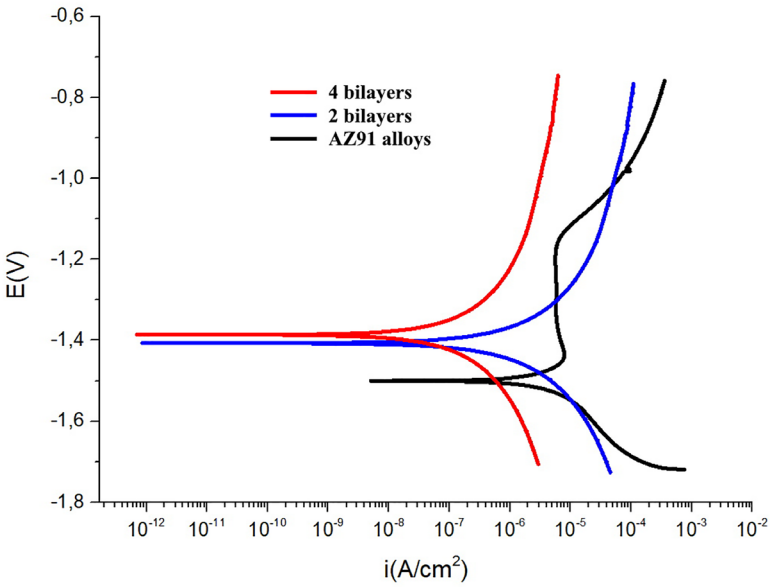

Figure 5: Potentiodynamic polarization curves of uncoated and multilayer film-coated AZ91 alloys immersed in artificial seawater.

The corrosion current density (I_{corr}) and corrosion potential (E_{corr}) derived from Tafel polarization curves are presented in Table 3. Moreover, the polarization resistances (R_p) of the uncoated and multilayer film-coated samples were calculated using the typical Stern–Geary equation [29]. According to the outcomes, the E_{corr} values of the multilayer coatings are higher, and the I_{corr} values are lower compared to the uncoated AZ91 alloys. This is because the coatings are a barrier for the substrate material against corrosion damage. Also, the highest E_{corr} value and the lowest I_{corr} value were taken from the multilayer sample coated with 4 bilayers. It could be explained that the influence of the grain size plays an essential role in the corrosion performance of multilayer coatings. The grain boundary acts as a physical corrosion barrier. A smaller grain size results in more grain boundaries, thereby reducing the corrosion rate in a microstructure with a smaller average grain size than a microstructure with coarser grains [26].

The electrochemical impedance measurements were used to compare the electrochemical properties of the uncoated and multilayer film-coated AZ91 alloys. Nyquist plots are shown in Figure 6, and the corresponding Bode plots are displayed in Figure 7. According to Figure 6, the Nyquist plots for the uncoated and all multilayer films are finished capacitance arcs. Moreover, the finished capacitance arc improved due to the grain size decrease; the highest capacitance arc value was obtained from the multilayer sample coated with 4 bilayers. Figure 7 displays the corresponding Bode plots. The corrosion resistance of the uncoated and multilayer film-coated alloys was evaluated by the model value of the impedance (|Z|) and the phase value. The higher values for both were observed in multilayer coatings, and it is known that a higher value of |Z| and phase angle stand for a more protective coating [30]. It may be observed that the maximal value of |Z| and the phase angle are both higher for the multilayer films compared to uncoated alloys, as shown in Figure 7.

Furthermore, the impedance |Z| value and phase angle increased with the increment in the number of bilayers. It could be explained that the highest impedance |Z| and phase angle values were observed in a multilayer sample coated with 4 bilayers. The circuit diagram described in Figure 8 was used to analyze the empirical data acquired from this system. Figure 8a illustrates the uncoated alloy's equivalent circuit, which exhibits a single time constant. A constant phase element (CPE) is used instead of pure capacitance to represent the inhomogeneous surface better, ensuring perfect compatibility in the fitting process. The circuit model (Figure 8a)

Table 3: Corrosion parameters and polarization resistance (R_p) determined from the tafel extrapolation method.

SAMPLES	E_{corr} (V)	I_{corr} (A/cm²)	b_a (V/dec)	b_c (V/dec)	R_p (kΩcm²)
AZ91 alloy	–1.52	3.81×10^{-7}	0.132	0.138	76.99
2 bilayers	–1.41	2.42×10^{-8}	0.113	0.117	106.45
4 bilayers	–1.36	3.81×10^{-9}	0.027	0.026	483.32

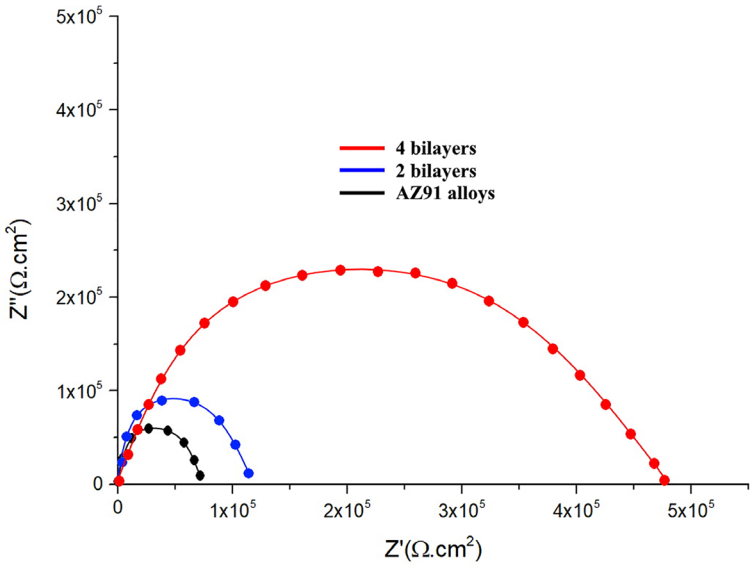

Figure 6: Nyquist plot obtained for uncoated and multilayer film-coated AZ91 alloys immersed in artificial seawater.

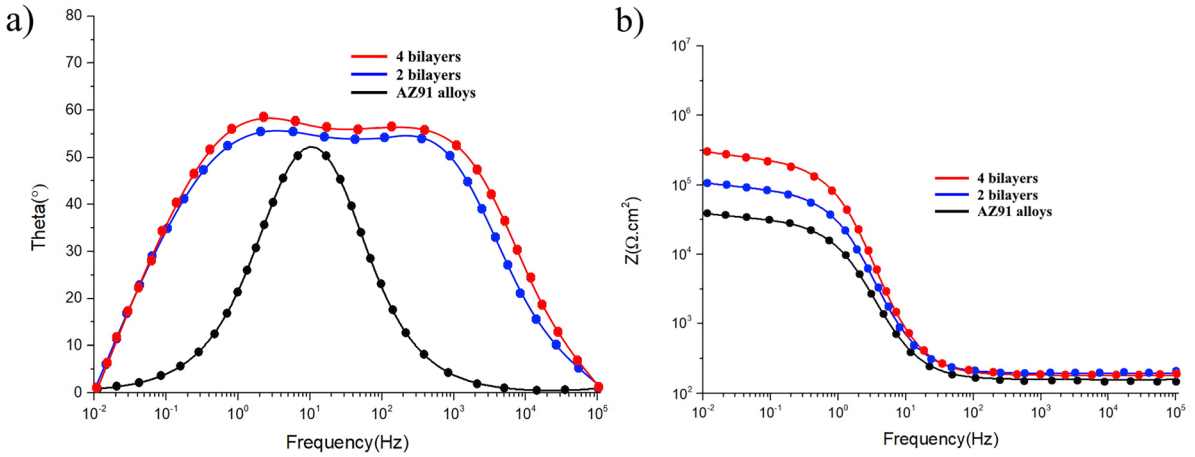

Figure 7: Bode plot obtained for uncoated and multilayer film-coated AZ91 alloys immersed in artificial seawater: Bode impedance (a) and bode phase angle (b).

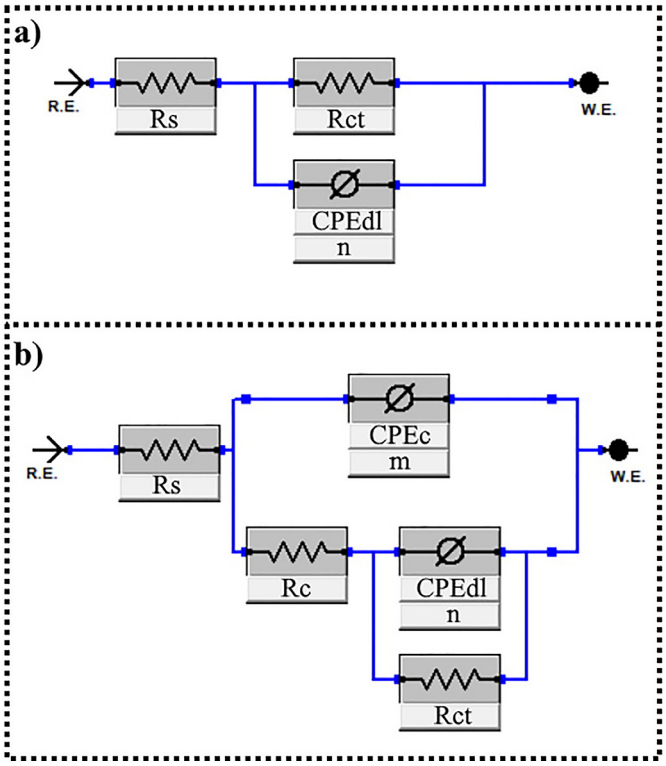

Figure 8: The equivalent electrical circuit of (a) uncoated and (b) multilayer film-coated AZ91 alloys.

comprises several components: R_s represents the resistance of artificial seawater, CPE_{dl} denotes the constant phase element of the double layer at the metal-artificial seawater interface, and R_{ct} signifies the charge transfer resistance of the AZ91 alloys. Fig.8b shows the equivalent electrical circuit of multilayer film-coated AZ91 alloys, offering three types of resistance (R) and two types of constant phase elements (CPE). They are: (1) resistance of the artificial seawater is characterized via the R_s, (2) the charge transfer at the multilayer film/alloys interface is characterized by the R_{ct}, (3) CPE_{dl} was signalized as the CPE of the interface between the multilayer system and the alloy, (4) the resistance of multilayer coating was indicated as CPEc represented Rc, (5) CPE of multilayer films. The total polarization resistance (R_t) is considered $R_t = R_s + R_{ct}$ for the uncoated AZ91 alloys and $R_t = R_s + R_{ct} + R_c$ for the coated samples [31]. Furthermore, Table 4 displays an increment in the R_t value after the multilayer film was formed on the surface of AZ91 alloys, compared with the uncoated alloys. This situation can be associated with the ability of multilayer films to provide resistance against corrosion by forming

Table 4: EIS results for all samples in artificial seawater.

SAMPLES	R_s ($\Omega.cm^2$)	R_c ($k\Omega.cm^2$)	CPE_c (S/cm^2s^n)	m	R_{ct} ($k\Omega.cm^2$)	CPE_{dl} (S/cm^2s^n)	n	R_t ($k\Omega.cm^2$)	$\chi 2$ chi-square
AZ91 alloy	71.5	–	–	–	66.333	4.8×10^{-8}	0.72	66.405	1.61×10^{-3}
2 bilayers	80.1	32.087	8.52×10^{-8}	0.65	80.582	3.1×10^{-8}	0.75	112.75	1.12×10^{-3}
4 bilayers	79.4	70.552	8.29×10^{-8}	0.67	425.478	2.3×10^{-8}	0.77	496.11	1.09×10^{-3}

a barrier between the substrate and the corrosive environment. Of all the samples coated with multilayer films, the sample with 4 bilayers exhibited the best corrosion resistance performance. It can be established that the contact angle measurement data corroborates the hydrophobic corrosion resistance results. The contact angles for the multilayer samples coated with 2 and 4 bilayers were 116° and 125°, respectively. This demonstrates that multilayer samples coated with 8 bilayers provide the best hydrophobic, water-repellent coating to prevent corrosion. Furthermore, these results indicate that the multilayer films with 8 bilayers exhibit strong corrosion resistance in corrosive environments.

4. CONCLUSIONS

Using the PVD coating technique, BN/TiO_2 multilayer films were deposited onto AZ91 alloys. Our findings revealed that, while Mg phase peaks were detected on uncoated alloy surfaces, BN-boron nitride and TiO_2-titanium dioxide peaks were found using diffraction from multilayer film-coated alloys according to XRD outcomes. Additionally, the intensity of the BN and TiO_2 peaks progressively decreased as the number of bilayers increased, and the shift of these peaks towards higher angles was assumed to be driven by compressive residual stresses in multilayered coating systems. The contact angles of the multilayer samples coated with 2 and 4 bilayers were 116° and 125°, respectively. This shows that multilayer samples coated with 8 bilayers had the optimum hydrophobic, water-repellent coating. The potentiodynamic polarization and EIS results revealed that BN/TiO_2 multilayer films exhibited superior corrosion resistance to uncoated alloys in artificial seawater. All of the coated samples had good corrosion resistance compared to uncoated AZ91, and their exceptional performance in synthetic saltwater was attributed to the multilayer coatings. This behavior can be attributed to the smaller grain size, increased layered interfaces, higher structural density, and better hydrophobic surface property.

5. BIBLIOGRAPHY

[1] GUO, J., CUI, X.-L., ZHAO, W., *et al*., "The tensile deformation behavior of AZ31B magnesium alloy sheet under intermittent pulse current", *Proceedings of the Institution of Mechanical Engineers. Part C, Journal of Mechanical Engineering Science*, v. 236, n. 1, pp. 471–480, 2022. doi: http://doi.org/10.1177/09544062211024280.

[2] YANG, L., WANG, Y., XU, W., *et al*., Research on marine atmospheric corrosion behavior of AZ31 magnesium alloy based on scientific ocean voyage. 2022. Preprint. doi: http://doi.org/10.21203/rs.3.rs-1706531/v1.

[3] WANG, D., PEI, S., WANG, Y., *et al*., "Effect of magnesium-to-phosphate ratio on the corrosion resistance of magnesium alloy embedded in magnesium potassium phosphate cement", *Cement and Concrete Composites*, v. 135, pp. 104826, 2023. doi: http://doi.org/10.1016/j.cemconcomp.2022.104826.

[4] LV, X., DENG, K.-K., WANG, C.-J., *et al*., "The corrosion properties of AZ91 alloy improved by the addition of trace submicron SiCp", *Materials Chemistry and Physics*, v. 286, pp. 126143, 2022. doi: http://doi.org/10.1016/j.matchemphys.2022.126143.

[5] YANG, L., LIN, C., GAO, H., *et al*., "Corrosion behaviour of AZ63 magnesium alloy in natural seawater and 3.5 wt.% NaCl aqueous solution", *International Journal of Electrochemical Science*, v. 13, n. 8, pp. 8084–8093, 2018. doi: http://doi.org/10.20964/2018.08.32.

[6] LI, J., LIU, X., ZHANG, J., *et al*., "Effects of inorganic metabolites of sulphate-reducing bacteria on the corrosion of AZ31B and AZ63B magnesium alloy in 3.5 wt.% NaCl solution", *Materials (Basel)*, v. 15, n. 6, pp. 2212, 2022. doi: http://doi.org/10.3390/ma15062212. PubMed PMID: 35329663.

[7] SONG, W., MARTIN, H.J., HICKS, A., *et al*., "Corrosion behaviour of extruded AM30 magnesium alloy under salt-spray and immersion environments", *Corrosion Science*, v. 78, pp. 353–368, 2014. doi: http://doi.org/10.1016/j.corsci.2013.10.020.

[8] ESMAILY, M., SVENSSON, J.E., FAJARDO, S., *et al*., "Fundamentals and advances in magnesium alloy corrosion", *Progress in Materials Science*, v. 89, pp. 92–193, 2017. doi: http://doi.org/10.1016/j.pmatsci.2017.04.011.

[9] XIN, Y., HUO, K., TAO, H., *et al*., "Influence of aggressive ions on the degradation behavior of biomedical magnesium alloy in physiological environment", *Acta Biomaterialia*, v. 4, n. 6, pp. 2008–2015, 2008. doi: http://doi.org/10.1016/j.actbio.2008.05.014. PubMed PMID: 18571486.

[10] LIU, H., CAO, F., SONG, G.-L., *et al*., "Review of the atmospheric corrosion of magnesium alloys", *Journal of Materials Science and Technology*, v. 35, n. 9, pp. 2003–2016, 2019. doi: http://doi.org/10.1016/j.jmst.2019.05.001.

[11] MELETLIOGLU, E., SADELER, R., "Comparison of corrosion, tribocorrosion and antibacterial properties of silver coatings on Ti15Mo by magnetron sputtering", *Surface Review and Letters*, v. 30, n. 05, pp. 2350027, 2023. doi: http://doi.org/10.1142/S0218625X23500270.

[12] ÇOMAKLI, O., "Improved structural, mechanical, corrosion and tribocorrosion properties of Ti45Nb alloys by TiN, TiAlN monolayers, and TiAlN/TiN multilayer ceramic films", *Ceramics International*, v. 47, n. 3, pp. 4149–4156, 2021. doi: http://doi.org/10.1016/j.ceramint.2020.09.292.

[13] MARIN, E., LANZUTTI, A., GUZMAN, L., *et al*., "Chemical and electrochemical characterization of TiO_2/Al_2O_3 atomic layer depositions on AZ-31 magnesium alloy", *Journal of Coatings Technology and Research*, v. 9, n. 3, pp. 347–355, 2012. doi: http://doi.org/10.1007/s11998-011-9372-8.

[14] STAIŠIŪNAS, L., MIEČINSKAS, P., LEINARTAS, K., *et al*., "Sputter-deposited Mg-Al-Zn-Cr alloys-Electrochemical characterization of single films and multilayer protection of AZ31 magnesium alloy", *Corrosion Science*, v. 80, pp. 487–493, 2014. doi: http://doi.org/10.1016/j.corsci.2013.11.061.

[15] WU, G., ZENG, X., LI, G., *et al*., "Preparation and characterization of ceramic/metal duplex coatings deposited on AZ31 magnesium alloy by multi-magnetron sputtering", *Materials Letters*, v. 60, n. 5, pp. 674–678, 2006. doi: http://doi.org/10.1016/j.matlet.2005.09.066.

[16] LIANG, F., SHEN, Y., PEI, C., *et al*., "Microstructure evolution and corrosion resistance of multi interfaces Al-TiAlN nanocomposite films on AZ91D magnesium alloy", *Surface and Coatings Technology*, v. 357, pp. 83–92, 2019. http://doi.org/10.1016/j.surfcoat.2018.09.019.

[17] ZHANG, D., QI, Z., WEI, B., *et al*., "Anticorrosive yet conductive Hf/Si3N4 multilayer coatings on AZ91D magnesium alloy by magnetron sputtering", *Surface and Coatings Technology*, v. 309, pp. 12–20, 2017. doi: http://doi.org/10.1016/j.surfcoat.2016.11.042.

[18] LI, H., LIU, X., ZHANG, C., *et al*., "Friction and wear properties of silicon nitride-based composites with different hbn content sliding against polyether-etherketone at different speeds under artificial seawater lubrication", *Coatings*, v. 12, n. 3, pp. 411, 2022. doi: http://doi.org/10.3390/coatings12030411.

[19] MORENO, H., CAICEDO, J.C., AMAYA, C., *et al*., "Enhancement of surface mechanical properties by using TiN [BCN/BN] n/c-BN multilayer system", *Applied Surface Science*, v. 257, n. 3, pp. 1098–1104, 2010. doi: http://doi.org/10.1016/j.apsusc.2010.08.024.

[20] TIAN, Y., ZHANG, X., SU, Z., *et al*., "Ultra-high-efficiency corrosion protection of metallic surface based on thin and dense hexagonal boron nitride coating films", *Langmuir*, v. 40, n. 13, pp. 7139–7146, 2024. doi: http://doi.org/10.1021/acs.langmuir.4c00272. PubMed PMID: 38504400.

[21] SHARMA, S., SHARMA, K., ROSMI, M.S., *et al*., "Morphology-controlled synthesis of hexagonal boron nitride crystals by chemical vapor deposition", *Crystal Growth & Design*, v. 16, n. 11, pp. 6440–6445, 2016. doi: http://doi.org/10.1021/acs.cgd.6b01110.

[22] ÇOMAKLI, O., YAZICI, M., KOVACI, H., *et al*., "Tribological and electrochemical properties of TiO2 films produced on Cp-Ti by sol-gel and SILAR in bio-simulated environment", *Surface and Coatings Technology*, v. 352, pp. 513–521, 2018. doi: http://doi.org/10.1016/j.surfcoat.2018.08.056.

[23] DEARNLEY, P., DAHM, K., ÇIMENOĞLU, H., "The corrosion-wear behaviour of thermally oxidised CP-Ti and Ti-6Al-4V", *Wear*, v. 256, n. 5, pp. 469–479, 2004. doi: http://doi.org/10.1016/S0043-1648(03)00557-X.

[24] WHITE, L., KOO, Y., YUN, Y., *et al*., "TiO_2 deposition on AZ31 magnesium alloy using plasma electrolytic oxidation", *Journal of Nanomaterials*, v. 2013, pp. 11–11, 2013. doi: http://doi.org/10.1155/2013/319437.

[25] LOPEZ-ORTEGA, A., BAYÓN, R., ARANA, J.L., *et al*., "Influence of temperature on the corrosion and tribocorrosion behaviour of High-Strength Low-Alloy steels used in offshore applications", *Tribology International*, v. 121, pp. 341–352, 2018. doi: http://doi.org/10.1016/j.triboint.2018.01.049.

[26] ÇOMAKLI, O., YAZICI, M., DEMIR, M., *et al*., "Effect of bilayer numbers on structural, mechanical, tribological and corrosion properties of TiO_2-SiO_2 multilayer film-coated β-type Ti45Nb alloys", *Ceramics International*, v. 49, n. 2, pp. 3007–3015, 2023. doi: http://doi.org/10.1016/j.ceramint.2022.09.285.

[27] ZHOU, D., PENG, H., ZHU, L., *et al*., "Microstructure, hardness and corrosion behaviour of Ti/TiN multilayer coatings produced by plasma activated EB-PVD", *Surface and Coatings Technology*, v. 258, pp. 102–107, 2014. doi: http://doi.org/10.1016/j.surfcoat.2014.09.058.

[28] SURMENEVA, M., NIKITYUK, P., HANS, M., *et al*., "Deposition of ultrathin nano-hydroxyapatite films on laser micro-textured titanium surfaces to prepare a multiscale surface topography for improved surface wettability/energy", *Materials (Basel)*, v. 9, n. 11, pp. 862, 2016. doi: http://doi.org/10.3390/ma9110862. PubMed PMID: 28773985.

[29] ÇOMAKLI, O., YAZICI, M., YETIM, T., *et al*., "Tribological and electrochemical behavior of Ag_2O/ZnO/NiO nanocomposite coating on commercial pure titanium for biomedical applications", *Industrial Lubrication and Tribology*, v. 71, n. 10, pp. 1166–1176, 2019. doi: http://doi.org/10.1108/ILT-11-2018-0414.

[30] SHEN, F., TAO, W., LI, L., *et al*., "Effect of microstructure on the corrosion resistance of coatings by extreme high speed laser cladding", *Applied Surface Science*, v. 517, pp. 146085, 2020. doi: http://doi.org/10.1016/j.apsusc.2020.146085.

[31] ACAR, M.T., ÇOMAKLI, O., YAZICI, M., *et al*., "The effect of doping different amounts of boron on the corrosion resistance and biocompatibility of TiO_2 nanotubes synthesized on SLM Ti6Al4V samples", *Surfaces and Interfaces*, v. 50, pp. 104472, 2024. doi: http://doi.org/10.1016/j.surfin.2024.104472.